Directional solidification, thermo-mechanical and optical properties of $(Mg_xCa_{1-x})_3Al_2Si_3O_{12}$ glasses doped with Nd^{3+} ions

D. Sola,[1,*] D. Conejos,[1] J. Martínez de Mendivil,[2] L. Ortega SanMartín,[3] G. Lifante,[2] and J. I. Peña[1]

[1]*Instituto de Ciencia de Materiales de Aragón, Universidad de Zaragoza-CSIC, Departamento de Ciencia y Tecnología de Materiales y Fluidos, C/ María de Luna 3, 50.018 Zaragoza, Spain*

[2]*Departamento de Física de Materiales, C-04, Facultad de Ciencias, Universidad, Autónoma de Madrid, Avda. Tomás y Valiente 7, 28.049 Madrid, Spain*

[3]*Departamento Sección Química, Pontificia Universidad Católica del Perú, Av. Universitaria 1801, San Miguel, Lima 32, Perú*

**dsola@unizar.es*

Abstract: In this work glass rods of $(Mg_xCa_{1-x})_3Al_2Si_3O_{12}$ (x = 0, 0.5 and 1) doped with 1 wt% Nd_2O_3 were produced by the laser floating zone technique. Thermo-mechanical and spectroscopic properties have been evaluated. The three glass samples present good thermo-mechanical properties, with similar hardness, toughness and glass transition temperatures. The spectroscopic characterization shows spectral shifts in absorption and emission spectra. These spectral shifts together with Judd-Ofelt intensity parameters and ionic packing ratio have been used to investigate the local structure surrounding the Nd^{3+} ions and the covalency of the Nd-O bond. All obtained results agree and confirm the higher covalency of the Nd-O bond in the $Ca_3Al_2Si_3O_{12}$ glass.

OCIS codes: (160.5690) Rare-earth-doped materials; (300.6360) Spectroscopy, laser; (160.2750) Glass and other amorphous materials.

References and links

1. K. Hirao, T. Mitsuyu, J. Si, and J. Qiu, *Active Glass for Photonic Devices: Photoinduced Structures and their Application* (Springer-Verlag, 2001).
2. J. H. Campbel, J. S. Hayden, and A. J. Marker, "High-power solid-state lasers from a laser glass perspective," Int. J. Appl. Glass Sci. **2**(1), 3–29 (2011).
3. E. Snitzer, "Optical maser action of Nd^{+3} in a barium crown glass," Phys. Rev. Lett. **7**(12), 444–446 (1961).
4. E. M. Erbe and D. E. Day, "Properties of Sm_2O_3-Al_2O_3-SiO_2 glasses for in vivo applications," J. Am. Ceram. Soc. **73**(9), 2708–2713 (1990).
5. E. V. Uhlmann, M. C. Weinberg, N. J. Kreidl, L. L. Burgner, R. Zanoni, and K. H. Church, "Spectroscopic properties of rare-earth-doped calcium-aluminate-based glasses," J. Non-Cryst. Solids **178**, 15–22 (1994).
6. S. L. Lin and C. S. Hwang, "Structures of CeO_2-Al_2O_3-SiO_2 glasses," J. Non-Cryst. Solids **202**(1-2), 61–67 (1996).
7. M. L. Baesso, A. C. Bento, L. C. M. Miranda, D. F. de Souza, J. A. Sampaio, and L. A. O. Nunes, "Rare-earth doped low silica calcium aluminosilicate glasses for near and mid infrared applications," J. Non-Cryst. Solids **276**(1-3), 8–18 (2000).
8. J. Marchi, D. S. Morais, J. Schneider, J. C. Bressiani, and A. H. A. Bressiani, "Characterization of rare earth aluminosilicate glasses," J. Non-Cryst. Solids **351**(10-11), 863–868 (2005).
9. A. Steimacher, M. J. Barboza, A. M. Farias, O. A. Sakai, J. H. Rohling, A. C. Bento, M. L. Baesso, A. N. Medina, and C. M. Lepienski, "Preparation of Nd_2O_3-doped calcium aluminosilicate glasses and thermo-optical and mechanical characterization," J. Non-Cryst. Solids **354**(42-44), 4749–4754 (2008).
10. L. Mota, J. A. Sampaio, M. G. da Silva, and H. Vargas, "Assessment of nonradiative relaxation time and characteristic diffusion time of neodymium, erbium and cobalt doped low silica calcium aluminosilicate glasses," Chem. Phys. Lett. **502**(1-3), 69–71 (2011).
11. A. Prnova, A. Domanicka, R. Klement, J. Kraxner, M. Polovka, M. Pentrak, D. Galusek, P. Simurka, and J. Kozankova, "Er- and Nd-doped yttrium aluminosilicate glasses: preparation and characterization," Opt. Mater. **33**(12), 1872–1878 (2011).

#239926 Received 29 Apr 2015; revised 15 Jun 2015; accepted 16 Jun 2015; published 30 Sep 2015

12. M. J. Weber, "Science and technology of laser glass," J. Non-Cryst. Solids **123**(1-3), 208–222 (1990).
13. R. R. Jacobs and M. J. Weber, "Dependence of the $^4F_{3/2} \rightarrow {}^4I_{11/2}$ induced-emission cross section for Nd^{3+} on glass composition," IEEE J. Quantum Electron. **QE-12**, 102–111 (1976).
14. F. R. Boyd and J. L. England, *Pyrope* (Carnegie Institution of Washington, 1959).
15. F. R. Boyd, J. L. England, and B. T. C. Davids, "Effects of pressure on the melting and polymorphism of Enstatite, $MgSiO_3$," J. Geophys. Res. **69**(10), 2101–2109 (1964).
16. T. Irifune and E. Ohtani, "Melting of Pyrope $Mg_3Al_2Si_3O_{12}$ up to 10 GPa: possibility of a pressure-induced structural change in Pyrope melt," J. Geophys. Res. **91**(B9), 9357–9366 (1986).
17. J. Ganguly, W. Cheng, and H. StC. O'Neill, "Syntheses, volume, and structural changes of garnets in the pyrope-grossular join: implications for stability and mixing properties," Am. Mineral. **78**, 583–593 (1993).
18. J. Zhang and C. Herzberg, "Melting Pyrope, $Mg_3Al_2Si_3O_{12}$ at 7-16 GPa," Am. Mineral. **79**, 497–503 (1994).
19. S. Greaux, N. Nishiyama, Y. Kono, L. Gautron, H. Ohfuji, T. Kunimoto, N. Menguy, and T. Irifune, "Phase transformations of $Ca_3Al_2Si_3O_{12}$ grossular garnet to the depths of the Earth's mantle transition zone," Phys. Earth Planet. Inter. **185**(3-4), 89–99 (2011).
20. E. Glezer and E. Mazur, "Ultrafast-laser driven micro-explosions in transparent materials," Appl. Phys. Lett. **71**(7), 882–884 (1997).
21. E. G. Gamaly, S. Juodkazis, K. Nishimura, H. Misawa, B. Luther-Davis, L. Hallo, P. Nicolai, and V. Tikhonchuk, "Laser-matter interaction in the bulk of a transparent solid: Confined microexplosion and void formation," Phys. Rev. B **73**, 214101 (2006).
22. A. Vailionis, E. G. Gamaly, V. Mizeikis, W. Yang, A. V. Rode, and S. Juodkazis, "Evidence of superdense aluminium synthesized by ultrafast microexplosion," Nat. Commun. **2**, 445–451 (2011).
23. J. Llorca and V. M. Orera, "Directionally solidified eutectic ceramic oxides," Prog. Mater. Sci. **51**(6), 711–809 (2006).
24. D. Sola, F. J. Ester, P. B. Oliete, and J. I. Peña, "Study of the stability of the molten zone and the stresses induced during the growth of Al_2O_3–$Y_3Al_5O_{12}$ eutectic composite by the laser floating zone technique," J. Eur. Ceram. Soc. **31**(7), 1211–1218 (2011).
25. F. J. Ester, D. Sola, and J. I. Peña, "Thermal stresses in the Al_2O_3-ZrO_2 (Y_2O_3) eutectic composite during the growth by the laser floating zone technique," Bol. Soc. Esp. Ceram. **47**, 352–357 (2008).
26. A. Solomah, *Indentation Techniques in Ceramic Materials Characterization: Theory and Practice* (Ceramic Transactions, 2003).
27. G. Padmaja and P. Kistaiah, "Optical characterization of Mn^{2+}: Li_2O-K_2O-CdO-B_2O_3 glass system: absorption edge, optical band gap, optical polarizability and optical basicity," IOP Conf. Series: Mat. Sci. and Eng. **2**, 012040 (2009).
28. M. J. Weber, "Glass for Neodymium glasses," J. Non-Cryst. Solids **42**(1-3), 189–196 (1980).
29. Y. Nageno, H. Takebe, and K. Morinaga, "Correlation between radiative transition probabilities of Nd^{3+} and composition in silicate, borate, and phosphate glasses," J. Am. Ceram. Soc. **76**(12), 3081–3086 (1993).
30. H. Takebe, Y. Nageno, and K. Morinaga, "Compositional dependence of Judd-Ofelt parameters in silicate, borate, and phosphate glasses," J. Am. Ceram. Soc. **78**(5), 1161–1168 (1995).
31. D. E. Henrie and G. R. Chopin, "Environmental effects on f-f transitions. III. Hypersensitivity in some complexes of trivalent Neodymium," J. Chem. Phys. **49**(2), 477–481 (1968).
32. B. R. Judd, "Optical absorption intensities of rare-earth ions," Phys. Rev. **127**(3), 750–761 (1962).
33. G. S. Ofelt, "Intensities of crystal spectra of rare-earth ions," J. Chem. Phys. **37**(3), 511–520 (1962).
34. J. H. Choi, A. Margaryan, A. Margaryan, and F. G. Shi, "Judd–Ofelt analysis of spectroscopic properties of Nd^{3+}-doped novel fluorophosphate glass," J. Lumin. **114**(3-4), 167–177 (2005).
35. W.T. Carnall, H. Crosswhite, and H.M. Crosswhite, *Energy Level Structure and Transition Probabilities in the Spectra of the Trivalent Lanthanides in LaF_3* (Argonne National Laboratory Rept. No ANL-78-XX-95, 1978).
36. T. Izumitani, H. Toratani, and H. Kuroda, "Radiative and nonradiative properties of Neodymium doped silicate and phosphate glasses," J. Non-Cryst. Solids **47**(1), 87–99 (1982).
37. W. F. Krupke, "Induced-emission cross sections in Neodymium laser glasses," IEEE J. Quantum Electron. **QE-10**(4), 450–457 (1974).
38. M. J. Weber, D. C. Ziegler, and C. A. Angell, "Tailoring stimulated emission cross sections of Nd^{3+} laser glass: observation of large cross sections for $BiCl_3$ glasses," J. Appl. Phys. **53**(6), 4344–4350 (1982).
39. S. Tanabe, T. Ohyagi, N. Soga, and T. Hanada, "Compositional dependence of Judd-Ofelt parameters of Er^{3+} ions in alkali-metal borate glasses," Phys. Rev. B Condens. Matter **46**(6), 3305–3310 (1992).
40. S. Tanabe, T. Hanada, T. Ohyagi, and N. Soga, "Correlation between ^{151}Eu Mössbauer isomer shift and Judd-Ofelt Ω_6 parameter of Nd^{3+} ions in phosphate and silicate laser glasses," Phys. Rev. B **48**(14), 3081–3086 (1993).
41. H. Takebe, Y. Nageno, and K. Morinaga, "Effect of network modifier on spontaneous emission probabilities of Er^{3+} in oxide glasses," J. Am. Ceram. Soc. **77**(8), 2132–2136 (1994).
42. H. Ebendorff-Heidepriem, D. Ehrt, M. Bettinelli, and A. Speghini, "Effect of glass composition on Judd-Ofelt parameters and radiative decay rates of Er^{3+} in fluoride phosphate and phosphate glasses," J. Non-Cryst. Solids **240**(1-3), 66–78 (1998).
43. R. D. Shannon, "Revised effective ionic radii and systematic studies of interatomic distances in halides and chalcogenides," Acta Crystallogr. A **32**(5), 751–767 (1976).
44. L. A. Riesberg and M. J. Weber, "Relaxation phenomena in rare-earth luminescence," Prog. Optics **14**, 89–159 (1975).

#239926 Received 29 Apr 2015; revised 15 Jun 2015; accepted 16 Jun 2015; published 30 Sep 2015

45. C. Brecher, L. A. Riesberg, and M. J. Weber, "Line-narrowed fluorescence spectra and site-dependent transition probabilities of Nd^{3+} in oxide and fluoride glasses," Phys. Rev. B **18**(10), 5799–5811 (1978).

1. Introduction

Lanthanide ion doped glasses have great interest for their use in telecommunication systems as glass fibers lasers, and optical amplifiers. In particular, the search for developing new solid-state lasers based on rare-earth (RE)-doped glass matrices is nowadays the subject of intense research [1,2]. The investigation of new laser wavelengths or new RE-doped glass matrices thus becomes a prior requirement in order to satisfy the demand of further outcomings in the development of this kind of solid-state lasers.

Since the first report on laser action in glass [3], many different glass compositions have been used (silicates, phosphates, fluorides) as matrix materials for trivalent rare-earth ions to produce active optical devices. Among them, rare-earth aluminosilicate and calcium aluminosilicate glasses have been studied for many years due to their high elastic modulus and hardness, high refraction index, high thermal conductivity, high glass transition temperature, excellent optical properties and good corrosion resistance [4–11]. Moreover, they are known for their ability to accommodate high concentration of rare-earth active ions such as Nd^{3+} or Er^{3+} as well as their low phonon energy due to the aluminate network. These properties have led to various applications in solid state lasers, optical waveguides, luminescence probes, and even in medicine as *in vivo* radiation delivery vehicles for cancer treatment of internal organs [4].

Among the possible rare-earth ions, neodymium has been studied in a large variety of glasses due to its potential applications in the field of infrared optical amplification related to the radiative efficiency of the $^4F_{3/2} \rightarrow {}^4I_{11/2}$ emission at around 1.06 μm [12]. In addition, the properties observed for Nd^{3+}, related to the modification in composition and microstructure, are also applicable to other rare-earths. It is well known that spectroscopic properties of trivalent rare-earth ion depend on the chemical composition of the glass matrix, which determines the structure and nature of the bonds [12,13].

The aim of this work is to assess thermo-mechanical and spectroscopic properties of neodymium doped $(Mg_xCa_{1-x})_3Al_2Si_3O_{12}$ glasses, for x = 0, 0.5 and 1, produced by the laser floating zone technique (LFZ). These compounds always adopt an amorphous state when they are prepared at room pressure but at high pressure and temperature conditions these materials may form crystals. In fact, the end members of the solution (x = 0 and 1) can be found in nature as the well-known crystalline minerals of Grossular, $Ca_3Al_2Si_3O_{12}$ and Pyrope, $Mg_3Al_2Si_3O_{12}$, both adopting garnet structure. The temperatures and pressures required to acquire this crystalline structure range 1000 - 1400°C and 2.5 - 4 GPa, respectively [14,15]. These P-T conditions have been reproduced at lab-scale by means of hydrothermal and dry techniques using piston-cylinder and multi-anvil press devices, and Grossular and Pyrope garnets have been successfully prepared departing from glasses [16–19]. On the other hand, it was recently demonstrated that it is possible to create extreme pressure and temperature conditions in table-top laboratory experiments with ultrashort laser pulses focussed inside transparent materials, with intensity in the focal spot significantly above the threshold for optical breakdown. These laser processing conditions transform the matter into a high-entropy state of dense plasma, a so called Warm Dense Matter (WDM), the state of matter in the core of planets and stars [20–22]. Tightly focalization of few femtosecond laser pulses can deposit energy densities of several $MJcm^{-3}$ into a submicron volume, several times higher than the strength of any material. This causes the solid to superheat yielding to the formation of plasma. This confined plasma explodes and generates a powerful shock wave that expands out of the focal volume and compresses the surrounding material. The shock wave of the expanding plasma can reach pressures of over 10 megabar (1 TPa), triggering dramatic changes in the material properties. The modified material remains confined in a strongly

#239926 Received 29 Apr 2015; revised 15 Jun 2015; accepted 16 Jun 2015; published 30 Sep 2015

localized region inside the unmodified surrounding bulk material so that it can be investigated later [20–22].

It is our aim to compare thermo-mechanical and spectroscopic results obtained in this work with laser synthesised optical glass-ceramics developed in a future work. These laser synthesised glass-ceramics are intended to be used as laser matrices since garnet structure is one of the most suitable materials to be used as active medium in optical amplification and solid-state lasers. In addition, the nature of these alkaline-earth aluminosilicate glasses have allow studying in the same glass network former, for the first time to the best of our knowledge, the local structure surrounding the Nd^{3+} ions and the covalence of the Nd-O bond related to the nephelauxetic effect in terms of absorption and emission spectral shifts, Judd-Ofelt intensity parameters and ionic packing ratio. All obtained results agree and confirm the higher covalency of the Nd-O bond in the Grossular glass.

2. Experimental

2.1 Samples fabrication

Glass rods were obtained by the laser floating zone technique (LFZ). This technique has been described in detail elsewhere [23]. The laser floating zone system includes a 600 W CO_2 semisealed laser (Electronic Engineering Blade 600) emitting at 10.6 μm and an in-house built growth chamber with gold coated metal mirrors for beam focussing, and two vertical axes for cylinder displacement. Both axes have independent rotation and translation movements. The mirror system inside the chamber consists of a reflaxicon that transforms the solid beam into a ring which is deflected by a flat mirror at 45° and focused on the ceramic rod by a parabolic mirror producing a homogenous heating. The correct optical alignment is obtained with the aid of a red diode laser coaxial with the infrared beam. Once the precursor is placed in the upper axis, the growth process starts by heating its lower end. When a drop is formed, a small seed placed in the lower axis is approached until a liquid bridge between the precursor and the seed is established. Then the seed is moved away while the precursor is moved towards the molten zone, and the volume of the liquid zone is kept constant. Identical feed and growth rates can be used when equal precursor and eutectic rod diameters are required. To increase or decrease the eutectic rod diameter, the growth rate must be lower or higher respectively than the precursor speed. The precursor and the grown rod are counter rotated to improve the heat distribution in the molten zone. This technique permits to control the solidification rate, providing high axial and radial thermal gradients in the liquid-solid interface, of paramount importance in the microstructure domain, and opens up the possibility of fabricating glasses and glass-ceramics samples [24,25].

Grossular, $Ca_3Al_2Si_3O_{12}$ (Ca-Glass), Pyrope, $Mg_3Al_2Si_3O_{12}$ (Mg-Glass) and the intermediate composition $Ca_{1.5}Mg_{1.5}Al_2Si_3O_{12}$ (CaMg-Glass) precursor rods were obtained by mixing stoichiometric amounts of Al_2O_3 (Sigma-Aldrich, 99.99%), SiO_2 (Aldrich, 99.6%), CaO (Aldrich, 99.9%) and MgO (Alfa, 99.5%) powders. Furthermore, 1 wt% of Nd_2O_3 (Aldrich, 99.99%) was added to the composites to obtain the doped samples. The resulting powders were isostatically pressed at 200 MPa for 3 minutes to obtain ceramic rods which were sintered at 1200°C for 12 hours.

2.2 Characterization techniques

Microstructure and composition were determined by means of field emission scanning electron microscopy (FESEM) using a Carl Zeiss Merlin equipped with an EDX detector. The amorphous character of the glass samples was analysed by X-ray powder diffraction (XRD) using a X´Pert Pro MPD diffractometer (Cu-kα radiation). Mechanical characterization was determined by a microhardness tester Matsuzawa MXT-70, and a nano-indenter Agilent Technologies G200. Thermogravimetric (TGA) and differential scanning calorimetry (DSC) tests were carried out using the SDT 600 Thermobalance from TA Instruments. Absorption

#239926 Received 29 Apr 2015; revised 15 Jun 2015; accepted 16 Jun 2015; published 30 Sep 2015

spectra were determined by using a 1050 Perkin Elmer spectrophotometer, and emission and excitation spectra were obtained by exciting the sample with a 3900S Spectra Physics Ti-sapphire. The fluorescence was analysed with a SpectraPro-500i monochromator. Lifetime measurements were obtained by exciting the samples with a pulsed Ti-sapphire laser and recording the decay times with an oscilloscope. Density was measured by Archimedes method and refractive index by dark mode technique.

3. Results and discussion

3.1 Compositional and microstructural characterization

Semi-quantitative chemical composition analysis of the glass samples was realised by EDX microanalysis to verify that the composition of the processed samples was around the theoretical composition. Table 1 shows the amount of oxides present in each sample. Composition of the samples was close to the nominal value. The amorphous nature of the samples was confirmed by XRD.

Table 1. Theoretical (T) and experimental composition (E) of the ceramic glasses in at%.

Composite	Al_2O_3		SiO_2		CaO		MgO	
	T	E	T	E	T	E	T	E
$Mg_3Al_2Si_3O_{12}$	14.28	11.76	42.86	43.24	-	-	42.86	45
$Ca_{1.5}Mg_{1.5}Al_2Si_3O_{12}$	14.28	14.42	42.86	44.64	21.43	18.83	21.43	22.11
$Ca_3Al_2Si_3O_{12}$	14.28	15.1	42.86	45.76	42.86	39.14	-	-

3.2 Thermo-mechanical characterization

Table 2 presents the thermo-mechanical properties for the three glass samples. Mechanical properties were assessed in terms of Vickers hardness, HV, and toughness, K_{IC}. Furthermore, Young's elastic modulus was determined from nano-indentation tests. Vickers hardness tests performed in the three glasses showed hardness values ranging between 5.68 and 7.37 GPa. Toughness was evaluated indirectly by indentation method making direct measurements of crack lengths created by the diamond indenter during hardness test [26]. Recorded values were between 0.77 and 1.24 MPa $m^{1/2}$. Nano-indentation tests carried out on the three samples reported Young's modulus between 82.10 and 99.90 GPa. With regards to the thermal characterization, DTA analyses performed on the samples reported glass transition temperatures, Tg, and peak crystallization temperatures, Tc, between 795 and 823 °C, and 1095 and 1101 °C respectively. It is worth mentioning that Ca-Glass did not show peak crystallization temperature. The three samples showed similar thermo-mechanical properties, and in the same range of magnitude if compared to other aluminosilicate glasses [7,9,11].

Table 2. Mechanical and thermal properties of $Ca_3Al_2Si_3O_{12}$, $Ca_{1.5}Mg_{1.5}Al_2Si_3O_{12}$ and $Mg_3Al_2Si_3O_{12}$ glasses.

Composite	HV (GPa)	K_{IC} (MPa $m^{1/2}$)	Young's Modulus (GPa)	Tg (°C)	Tc (°C)
$Ca_3Al_2Si_3O_{12}$	6.17 ± 0.24	0.77 ± 0.17	94.40 ± 0.80	823 ± 2	-
$Ca_{1.5}Mg_{1.5}Al_2Si_3O_{12}$	5.68 ± 0.18	1.04 ± 0.29	82.10 ± 0.60	812 ± 2	1101 ± 1
$Mg_3Al_2Si_3O_{12}$	7.37 ± 0.22	1.24 ± 0.31	99.90 ± 1.50	795 ± 1	1095 ± 1

#239926 Received 29 Apr 2015; revised 15 Jun 2015; accepted 16 Jun 2015; published 30 Sep 2015

3.3 Optical characterization

3.3.1 Absorption properties

Room temperature absorption spectra were obtained for the three samples in the 200-1000 nm range. Figure 1 shows the absorption cross-section spectra as a function of wavelength for the glass samples doped with $1.049x10^{20}$, $1.014x10^{20}$ and $1.018x10^{20}$ at./cm^3 of Nd^{3+} ions for Ca-Glass, CaMg-Glass and Mg-Glass respectively. The absorption bands correspond to the 4f-4f optical excitations between the $^4I_{9/2}$ ground level and their excited states of the Nd^{3+} ions. The absorption spectra show an absorption edge shift to the UV range for the Ca-Glass with respect to the Mg-Glass which is related to the higher polarizability of the Ca^{2+} ions [27]. Worth noting is that the absorption edge of the intermediate glass is placed between the extreme compositions.

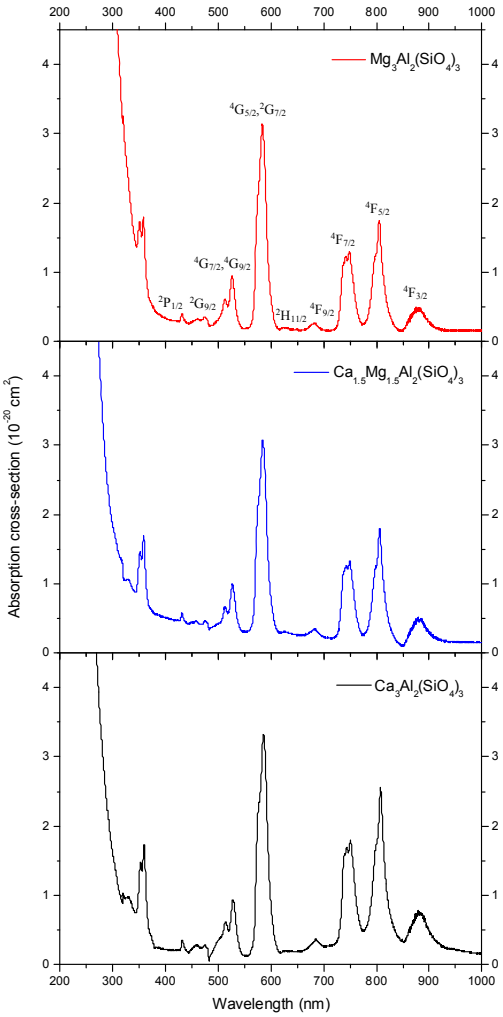

Fig. 1. Room temperature absorption cross-section spectra as a function of wavelength for $Ca_3Al_2Si_3O_{12}$, $Ca_{1.5}Mg_{1.5}Al_2Si_3O_{12}$ and $Mg_3Al_2Si_3O_{12}$ glasses doped with Nd^{3+} ions.

Generally speaking absorption and emission spectra of RE-doped glasses show spectral shifts which depend on the choice of the glass composition and the degree of covalent

#239926 Received 29 Apr 2015; revised 15 Jun 2015; accepted 16 Jun 2015; published 30 Sep 2015

bonding of the RE ion so that the spectroscopic properties of RE ions change with glass composition. Spectral shifts arise from the nephelauxetic or cloud expanding effect, where the red shift means an increase of the covalency related to the expansion of the 4f orbital cloud [28–30]. They are generally affected most by the glass network former. However, within a given glass composition, further variations are possible by the selection of the network-modifier cations [29,30].

The estimation of the covalency between the rare-earth ion and its ligand can be carried out by means of the shift of the absorption peak wavenumber of the 4f-4f transitions [30,31]. For this purpose and for the case of Nd^{3+}-doped glasses, the shift of the hypersensitive transition $^4I_{9/2}\rightarrow{}^4F_{7/2},{}^4S_{3/2}$ is selected. Conversely to other rare-earth hypersensitive transitions, $^4I_{9/2}\rightarrow{}^4F_{7/2},{}^4S_{3/2}$ transition of Nd^{3+} shows two peaks by the Stark splitting so that the peak wavenumber cannot be determined correctly. In this case, the relative intensity ratio between the peaks is used as covalency parameter of Nd^{3+}-ion sites since this ratio varies with glass composition [29,30]. Figure 2 shows the normalized $^4I_{9/2}\rightarrow{}^4F_{7/2},{}^4S_{3/2}$ absorption transition, where a spectral shift and a difference in the relative peak intensity ratio is observed. Peak intensities, designated as I_S and I_L, correspond to the peak intensities at the shortest and longest wavelengths. Increase of the ratio I_L/I_S indicates a shift of the centre of gravity of the absorption spectra to lower energies, i.e., longer wavelengths. This red shift means an increase in the covalency of the Nd-O bond [30]. In particular, the I_L/I_S ratio is 1.06 and 1.04 for the Ca-Glass and Mg-Glass respectively so that the covalency of the Nd-O bond is higher for the Ca-Glass than for the Mg-Glass.

3.3.2 Judd-Ofelt parameters and emission properties

The forced electric-dipole transition probability between 4f levels of rare-earth ion is estimated from absorption spectra on the basis of Judd-Ofelt theory [32,33]. Transition oscillator strengths can be experimentally determined from the optical absorption spectra using the equation

$$f_{exp} = \frac{mc^2}{\pi Ne^2}\int \frac{\alpha(\lambda)}{\lambda^2} d\lambda \qquad (1)$$

where m and e are the electron mass and charge respectively, c is the light velocity, $\alpha(\lambda)$ the optical absorption coefficient as a function of wavelength λ and N is the concentration of the absorbing ions. Table 3 shows such oscillator strengths for the three compositions at 300 K together with the assignment of the bands to particular transitions.

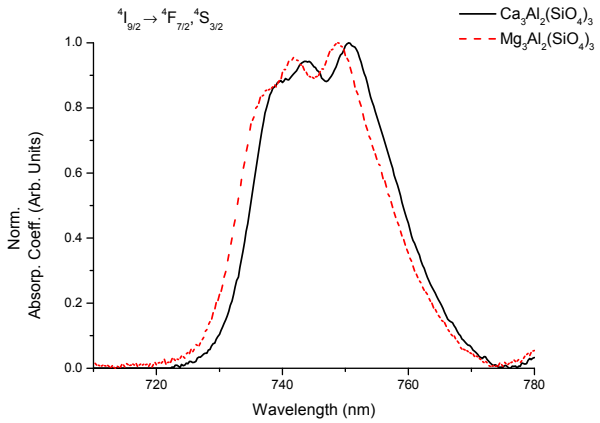

Fig. 2. Normalized $^4I_{9/2}\rightarrow{}^4F_{7/2},{}^4S_{3/2}$ absorption transition for $Ca_3Al_2Si_3O_{12}$, and $Mg_3Al_2Si_3O_{12}$ glasses doped with Nd^{3+} ions.

#239926 Received 29 Apr 2015; revised 15 Jun 2015; accepted 16 Jun 2015; published 30 Sep 2015

Table 3. Experimental (f_{exp}) and calculated (f_{cal}) oscillator strength of Nd^{3+} in $Ca_3Al_2(SiO_4)_3$, $Mg_3Al_2(SiO_4)_3$ and $Ca_{1.5}Mg_{1.5}Al_2(SiO_4)_3$ glasses.

	$Ca_3Al_2(SiO_4)_3$			$Ca_{1.5}Mg_{1.5}Al_2(SiO_4)_3$			$Mg_3Al_2(SiO_4)_3$		
Level	λ (nm)	f_{exp} (x10^{-6})	f_{cal} (x10^{-6})	λ (nm)	f_{exp} (x10^{-6})	f_{cal} (x10^{-6})	λ (nm)	f_{exp} (x10^{-6})	f_{cal} (x10^{-6})
$^4F_{3/2}$	880	2.42	3.59	880	1.95	2.31	880	1.60	2.56
$^4F_{5/2}$, $^2H_{9/2}$	807.75	7.81	8.15	806.25	5.94	6.00	805.5	5.74	6.16
$^4F_{7/2}$, $^4S_{3/2}$	750.5	6.83	6.81	749.25	5.46	5.48	748.75	5.45	5.33
$^4F_{9/2}$	684.5	0.53	0.58	683	0.50	0.45	683.25	0.45	0.45
$^4G_{5/2}$, $^2G_{7/2}$	586	22.37	22.38	584.75	19.40	19.40	583.75	19.93	19.93
$^2K_{13/2}$, $^4G_{7/2,9/2}$	528.5	7.93	7.03	527	5.09	4.75	526.25	6.10	5.15
$^2K_{15/2}$, $^2G_{9/2}$, $^2D_{3/2}$, $^4G_{11/2}$	474	2.49	1.71	474.75	1.09	1.17	473.25	1.24	1.26
$^2P_{1/2}$	432	0.55	0.11	431	0.39	0.72	431	0.40	0.81

According to the Judd-Ofelt theory, the oscillator strength *f (J, J')* of the $J \rightarrow J'$ transition occurring at the mean frequency ν is given by

$$f(J,J') = \frac{8\pi^2 m\nu}{3h(2J+1)e^2 n^2}\left[X_{ed}S_{ed} + X_{md}S_{md}\right] \quad (2)$$

where n is the refractive index, $X_{ed} = n(n^2 + 2)^2/9$ is the local field correction for electric-dipole transitions and $X_{md} = n^3$ for magnetic-dipole ones. Magnetic-dipole transitions give only a negligible contribution to the transition bands of Nd^{3+} so that they are not taken into account [34,35].

The electric-dipole strength is given by

$$S_{ed}(J,J') = e^2 \sum_{t=2,4,6} \Omega_t \left|\left\langle (S\,L)J \middle\| U^{(t)} \middle\| (S'L')J' \right\rangle\right|^2 \quad (3)$$

where Ω_2, Ω_4 and Ω_6 are the Judd-Ofelt, JO, intensity parameters. The reduced matrix elements $<\|U^{(t)}\|>$ are almost insensitive to the environment and the values provided by Carnall et al. have been used [35]. Intensity parameters Ω_2, Ω_4 and Ω_6, obtained by the least-squares method, are shown in Table 4 and compared to those obtained for other silicate glasses in which the alkali and alkaline-earth oxide modifiers have been exchanged between Li^+, Na^+, K^+ and Mg^{2+} and Ca^{2+} respectively. The calculated oscillator strength values are also compared to the experimental ones in Table 3.

The JO intensity parameters contain implicitly odd-symmetry crystal field terms, radial integrals, and perturbation denominators. These coefficients, regarded as phenomenological parameters, are usually used to evaluate spontaneous emission probability, induced-emission cross-section, quantum efficiency, and branching ratios. The close relationship between JO parameters and the nature of the glass host allows tailoring, within limits, these optical properties based on the suitable choice of the glass composition. JO parameters are related to local structures in the vicinity of rare-earth ions and/or the covalency of the rare-earth-ion site [12,13,28–30,36–42]. For instance, Ω_2 is sensitive to the local structures in the vicinity of rare-earth ions relating to the anion structures of host glasses and reflects the asymmetry around the rare-earth ions. However, the spontaneous emission probabilities are independent of Ω_2. On the other hand, Ω_6 is of particular interest because this parameter affects the values of the calculated spontaneous emission probabilities for the $^4F_{3/2} \rightarrow {}^4I_{11/2}$ transition of Nd^{3+}. The Ω_4 parameter is affected by the factors causing changes in both Ω_2 and Ω_6. Especially, if the changes of Ω_2 and Ω_6 are opposite, the resolution of the respective effects on Ω_4 is difficult. Therefore, Ω_2 and Ω_6 are mostly studied for local structure investigations [42]. With

#239926 Received 29 Apr 2015; revised 15 Jun 2015; accepted 16 Jun 2015; published 30 Sep 2015

regards to the Ω_6 parameter, this intensity parameter is insensitive to local structures but related to the covalency of the rare-earth-ion site [13,28–30,36–41]. Tanabe et al. stated that Ω_6 of Nd^{3+} and of Er^{3+} decreased with increasing the covalency of the rare-earth-ion sites in oxide glasses [39,40]. On the contrary, Takebe et al. reported that in silicate, borate and phosphate glasses Ω_6 of Nd^{3+} increased and Ω_6 of Er^{3+} decreased when the covalency between the rare-earth ion and the oxygen ion increased [29,30,41].

Table 4. Judd-Ofelt intensity parameters (in $10^{-20}cm^2$) for Nd^{3+} in $Ca_3Al_2(SiO_4)_3$, $Mg_3Al_2(SiO_4)_3$ and $Ca_{1.5}Mg_{1.5}Al_2(SiO_4)_3$ glasses.

	Ω_2	Ω_4	Ω_6	δ_{rms}	Reference
$Mg_3Al_2(SiO_4)_3$	5.40	3.56	3.78	1.99 x10^{-7}	This work
$Ca_{1.5}Mg_{1.5}Al_2(SiO_4)_3$	4.81	4.11	3.86	1.56 x10^{-7}	This work
$Ca_3Al_2(SiO_4)_3$	4.71	5.85	4.64	5.97 x10^{-7}	This work
$20Li_2O$-$20MgO$-$60SiO_2$	3.89	4.64	5.19		[29]
$20Li_2O$-$20CaO$-$60SiO_2$	3.63	4.21	4.94		[29]
$20Na_2O$-$20MgO$-$60SiO_2$	4.74	3.61	4.19		[29]
$20Na_2O$-$20CaO$-$60SiO_2$	4.64	3.81	4.17		[29]
$20K_2O$-$20MgO$-$60SiO_2$	5.71	3.36	2.57		[29]
$20K_2O$-$20CaO$-$60SiO_2$	5.23	3.10	3.14		[29]
$20Na_2O$-$15MgO$-$65SiO_2$	4.3	3.6	3.3		[36]
$20Na_2O$-$15CaO$-$65SiO_2$	4.3	4.0	3.7		[36]

Despite the numerous works on compositional dependence of intensity parameters, the correlation between intensity parameters and glass structure has not yet been completely clarified. As an example, Table 4 shows that Ω_2 increases in the order Ca < Mg independently of the alkali or Al_2O_3 network-modifier used. However, there is not any trend in the increasing order for Ω_4 and Ω_6. In the Ca-Glass and Mg-Glass studied in this work, Ω_4 and Ω_6 increase in the order Mg < Ca as in the silicate glasses reported by Izumitani et al. [36]. On the contrary, the values reported by Nageno et al. [29] show that there is not any pattern in the variation of Ω_4 and Ω_6 with the type of the alkali oxide. In the glasses with Li^+ and K^+ the increasing order for Ω_4 is Ca < Mg, but in the glass with Na^+ the increasing order is Mg < Ca. With regards to Ω_6, in Li^+ and Na^+ glasses the increasing order is Ca < Mg but the in glass with K^+ the increasing order is the contrary. Moreover, the increasing order for Ω_6 reported by Nageno et al. for Na^+ glasses mismatches the values reported by Izumitani et al. for the same glass system.

According to Nageno et al. Ω_2 is independent of the I_L/I_S intensity ratio, i.e., the covalency of the Nd-O bond. Furthermore, it is well known that Ω_2 is sensitive to local structure in the vicinity of Nd^{3+} ions. In this way, in ternary alkali alkaline-earth glasses, Ω_2 increases monotonically with increasing difference in the field strength between alkali and alkaline-earth ions. So the distortion in the vicinity of Nd^{3+} ions is increased due to the combination of alkali and alkaline-earth oxides, and as a result Ω_2 is increased. This behaviour is also observed in the Mg-Glass and Ca-Glass, as shown in Table 4, but in this case is due to the higher field strength between aluminate and Mg^{2+} ion.

On the other hand, Ω_6 behaviour is related to the covalency of the rare-earth-ion site in glasses. The absorption peak wavenumber of the transitions whose intensities are determined mainly by Ω_6, such as the $^4I_{9/2}\rightarrow{}^4F_{7/2},{}^4S_{3/2}$ for the Nd^{3+}, is shifted systematically with glass composition, due to the nephelauxetic effect. As seen in the previous section, the covalency of the Nd-O bond increased with increasing the intensity ratio I_L/I_S. Furthermore, according to

#239926 Received 29 Apr 2015; revised 15 Jun 2015; accepted 16 Jun 2015; published 30 Sep 2015

Takebe et al., Ω_6 increased with the covalency of the Nd-O bond. These results are in agreement for the JO parameters Ω_6 obtained in this work, since Ω_6 is higher for the Ca-Glass than for the Mg-Glass, as shown in Table 4 and hence the covalency of the Nd-O bond is higher for the Ca-Glass.

In addition, the covalency of the rare-earth-ion site can also be correlated to the ionic packing ratio, V_p, which can be expressed as [29]

$$V_P = \frac{\sum_i \frac{4}{3}\pi r_i^3 n_i N_A}{V_m} \tag{4}$$

where r_i is the ionic radius taken as the effective ionic radius $r(O^{2-}) = 0.138$ nm [43], n_i is the molar fraction, N_A is the Avogadro number, $V_m = M/\rho$ is the molar volume, M is the molar weight, and ρ is the density of the glass host. This calculation gives an ionic packing ratio V_P of 55.9% and 58.7% for the Mg-Glass and Ca-Glass respectively. The ionic packing ratio, which is a macroscopic property of a glass host, greatly affects Ω_6 and the spontaneous emission probabilities of Nd^{3+} and Er^{3+} in silicate and borate glasses [29,31]. In particular, Ω_6 parameter and the total spontaneous emission probability increase with increasing ionic packing ratio which corresponds to an increase in the covalency of the Nd-O bond. This result is also in agreement with the obtained in this work since V_P is higher for the Ca-Glass, confirming the higher covalency of the Nd-O in the Ca-Glass.

Once Ω_i are obtained, the evaluation of the system for optical applications in terms of radiative transition probabilities, emission branching ratios, radiative lifetimes, quantum efficiency and peak induced-emission cross-section can be carried out.

The radiative transition probability from the initial manifold $|(S,L)J\rangle$ to the terminal manifold $|(S',L')J'\rangle$ is given by

$$A_{rad}\left[(S,L)J;(S',L')J'\right] = \frac{64\pi^4}{3h(2J+1)\lambda^3}\left[\frac{n(n^2+2)^2}{9}\right]S_{ed} \tag{5}$$

Fluorescence branching ratios for transitions originating on a specific initial manifold $|(S,L)J\rangle$ are defined by

$$\beta\left[(S,L)J;(S',L')J'\right] = \frac{A_{rad}\left[(S,L)J;(S',L')J'\right]}{\sum_{S',L',J'} A_{rad}\left[(S,L)J;(S',L')J'\right]} \tag{6}$$

where the summation is over all terminal manifolds $|(S',L')J'\rangle$. The sum represents the total transition probability for radiative decay from the initial manifold. Obtained calculated values are listed in Table 5. Fluorescence branching ratio to $^4I_{11/2}$ level should be as favourable as possible in order to optimise laser action. Since intensity of $^4F_{3/2} \rightarrow {}^4I_{11/2}$ laser transition is dependent only on the Ω_4 and Ω_6 parameters because of the triangle rule [44], the branching ratio can be expressed in terms of the ratio Ω_4/Ω_6 so that the optimal intensity to $^4I_{11/2}$ level is obtained for the lower Ω_4/Ω_6 ratio [13]. For the Mg-Glass and Ca-Glass this ratio is 0.92 and 1.26 respectively. As consequence of the lower Ω_4/Ω_6 ratio for the Mg-Glass, the branching ratio to the $^4I_{11/2}$ level is higher than for the Ca-Glass, specifically a 47.7 and 44.5% respectively, Table 5.

#239926 Received 29 Apr 2015; revised 15 Jun 2015; accepted 16 Jun 2015; published 30 Sep 2015

Table 5. Radiative transitions probabilities and branching ratios of Nd^{3+} in $Ca_3Al_2(SiO_4)_3$, $Mg_3Al_2(SiO_4)_3$ and $Ca_{1.5}Mg_{1.5}Al_2(SiO_4)_3$ glasses.

	$Ca_3Al_2(SiO_4)_3$		$Ca_{1.5}Mg_{1.5}Al_2(SiO_4)_3$		$Mg_3Al_2(SiO_4)_3$	
$^4F_{3/2}$	A_{rad} (s^{-1})	β (%)	A_{rad} (s^{-1})	β (%)	A_{rad} (s^{-1})	β (%)
$^4I_{9/2}$	1613.3	47.5	1105.6	45.4	964.6	43.0
$^4I_{11/2}$	1512.7	44.5	1121.1	46.0	1070.3	47.7
$^4I_{13/2}$	259.6	7.6	200.7	8.2	200.0	8.9
$^4I_{15/2}$	12.6	0.4	9.7	0.4	9.7	0.4
Total	3398.1		2437.2		2244.5	

Radiative lifetime is related to the total radiative transition probabilities A_{rad} by its reciprocal

$$\tau_R = \left\{ \sum_{S',L',J'} A_{rad}\left[(S,L)J;(S',L')J'\right] \right\}^{-1} \tag{7}$$

obtaining values of 294, 410 and 445 μs for the Ca-Glass, CaMg-Glass and Mg-Glass respectively. The radiative quantum efficiency of the $|(S,L)J\rangle$ manifold defined as

$$\eta = \tau_f / \tau_R \tag{8}$$

where τ_f is the fluorescence lifetime, which is due to all relaxation processes, and was found to be 272, 261 and 273 μs for the Ca-Glass, CaMg-Glass and Mg-Glass respectively giving rise to quantum efficiencies of 0.93, 0.63 and 0.61 for the three compositions respectively. In this way, according to the previous results the higher the covalency of the rare-earth-ion site the shorter the radiative lifetime and the higher the quantum efficiency.

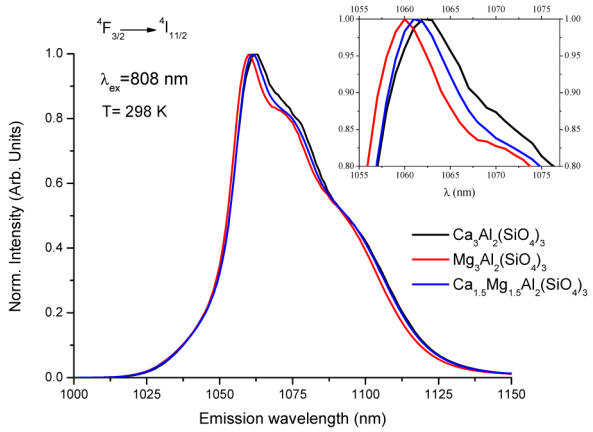

Fig. 3. Normalized fluorescence spectra of the $^4F_{3/2} \rightarrow {}^4I_{11/2}$ laser transition at room temperature measured by exciting the samples at 808 nm.

The $^4F_{3/2} \rightarrow {}^4I_{11/2}$ steady-state fluorescence spectra at room temperature were measured by exciting the samples at 808 nm in resonance with the $^4I_{9/2} \rightarrow {}^4F_{5/2}, {}^2H_{9/2}$ absorption band. Figure 3 shows the differences in the normalized emission spectra for the three samples in terms of fluorescence peak wavelength, λ_p, and effective bandwidth, $\Delta\lambda_{eff}$, the latter obtained by integrating the fluorescence band and dividing by the peak wavelength. The obtained fluorescence bands were inhomogeneously broadened due to site-to-site variations in the local field seen by rare-earth ions in the glass, and asymmetric, with a shift to high energy values in

#239926 Received 29 Apr 2015; revised 15 Jun 2015; accepted 16 Jun 2015; published 30 Sep 2015

the emission maximum for the Mg-Glass compared to Ca-Glass. These features yield to a shorter effective bandwidth, which is a measure of the overall extent of the Stark splitting of the J manifolds. In particular, Mg-Glass, CaMg-Glass and Ca-Glass peak wavelengths were placed at 1060, 1061 and 1062 nm, with effective bandwidths of 42, 43 and 44 nm respectively, Table 6.

Table 6. Room Temperature emission properties of Nd^{3+} in $Ca_3Al_2(SiO_4)_3$, $Mg_3Al_2(SiO_4)_3$ and $Ca_{1.5}Mg_{1.5}Al_2(SiO_4)_3$ glasses.

Sample	n	λ_p (nm)	$\Delta\lambda_{eff}$ (nm)	σ_p (x10^{-20} cm^2)
$Mg_3Al_2(SiO_4)_3$	1.579	1060	42	1.72
$Ca_{1.5}Mg_{1.5}Al_2(SiO_4)_3$	1.591	1061	43	1.73
$Ca_3Al_2(SiO_4)_3$	1.616	1062	44	2.24

The stimulated emission cross-section of the laser transition can be determined from spectral parameters and from the calculated radiative transition probability by making use of [13]

$$\sigma_P(\lambda_p) = \frac{\lambda_p^4}{8\pi c n^2 \Delta\lambda_{eff}} A\left[\left({}^4F_{3/2}\right);\left({}^4I_{11/2}\right)\right] \quad (9)$$

where λ_p is the fluorescence peak wavelength, n is the refractive index, $\Delta\lambda_{eff}$ is the effective bandwidth of the $^4F_{3/2}\rightarrow{}^4I_{11/2}$ transition, and $A[(^4F_{3/2});(^4I_{11/2})]$ is the radiative transition probability for this transition. The stimulated emission cross-sections for the $^4F_{3/2}\rightarrow{}^4I_{11/2}$ transition for the three samples are presented in Table 6. The higher cross-section of the Ca-Glass is because large emission cross-section requires Ω_4 and Ω_6 intensity parameters as large as possible and, as shown in Table 4, this glass has the largest intensity parameters. According to these results the higher the covalency of the rare-earth-ion site the higher effective bandwidth and emission cross-section. Furthermore, the estimation of the covalency between the rare-earth ion and its ligand can also be carried out by means of the peak wavelength shift of the fluorescence spectrum of Nd^{3+}. Jacobs and Weber studied the differences in the $^4F_{3/2}\rightarrow{}^4I_{11/2}$ fluorescence spectra for several glass network formers and network-modifier ions. They reported that the shift of the fluorescence peak wavelength to longer wavelengths was caused by the increase of the covalency between the Nd^{3+} ion and the oxygen ion in oxide glasses, i.e., the so called nephelauxetic effect. However, They did not find any variation in the fluorescence peak wavelength for alkaline-earth alkali ternary silicate glasses when the alkaline-earth additive was exchanged between Mg^{2+}, Ca^{2+}, Sr^{2+} and Ba^{2+} ions [13]. Furthermore, they found that the effective bandwidth decreased in the order Ca < Mg, conversely to the results found in this work, see Table 6. Brecher et al. also studied the correlation between the nephelauxetic effect with the fluorescence peak wavelength shift by comparing the fluorescence line narrowing spectra between oxide and fluoride glasses [45]. However, there have not been found previous works, to our best knowledge, in which the exchange of the alkaline-earth cations in the same glass network former had been used to explain the correlation between fluorescence peak shift and nephelauxetic effect. This work shows for the first time that in aluminosilicate network former the modification of the alkaline-earth network-modifier gives rise to a fluorescence peak wavelength shift so that it can be used to assess the covalency of the Nd-O bond. In particular, the red shift observed in the fluorescence peak wavelength for the Ca-Glass with regards to the Mg-Glass indicates the higher covalency of the Nd-O bond in the Ca-Glass, in good agreement with the results obtained in previous sections.

#239926 Received 29 Apr 2015; revised 15 Jun 2015; accepted 16 Jun 2015; published 30 Sep 2015

4. Conclusions

In this work $Ca_3Al_2Si_3O_{12}$, $Mg_3Al_2Si_3O_{12}$ and $Ca_{1.5}Mg_{1.5}Al_2Si_3O_{12}$ glasses doped with Nd^{3+} ions were grown by the laser floating zone technique. Thermo-mechanical and spectroscopic characterization were carried out in order to establish their properties as laser matrix and to used them as starting point before realizing laser synthesis processes in their inside.

The three glass samples showed good thermo-mechanical properties, with similar hardness, toughness and glass transition temperature, and in the same range when compared to other aluminosilicate glasses. Optical characterization revealed absorption and fluorescence spectral shifts arisen from the nephelauxetic effect. These spectral shifts together with Judd-Ofelt intensity parameters and ionic packing ratio were used to study the covalency of the Nd-O bond in the glass samples. The close relationship between intensity parameters and the nature of the glass host allowed evaluating the local structure surrounding the Nd^{3+} ions and the covalency of the Nd-O bond. The higher distortion in the vicinity of Nd^{3+} ions caused by the higher field strength between aluminate and Mg^{2+} ion was explained in terms of the increasing of Ω_2 intensity parameter. The higher values obtained for Ω_6 intensity parameter and ionic packing ratio in the $Ca_3Al_2Si_3O_{12}$ glass agree with the higher covalency of the Nd-O site in this glass. Emission properties were also calculated for the three glass samples. The higher the covalency of the rare-earth-ion site the shorter the radiative lifetime and the higher the quantum efficiency obtained. Furthermore, the broader effective bandwidth and the higher emission cross-section were also found in the $Ca_3Al_2Si_3O_{12}$ glass.

Acknowledgments

Daniel Sola thanks the Bosch and Siemens Home Appliances Group and the 7th Framework Programme EU No 314630-UV Marking for the financial support of his contract. Departamento de Ciencias (PUCP) is acknowledged for allowing the short stay of Luis Ortega-San-Martin at the University of Zaragoza.

#239926 Received 29 Apr 2015; revised 15 Jun 2015; accepted 16 Jun 2015; published 30 Sep 2015